Proceedings of ASME Turbo Expo 2020
Turbomachinery Technical Conference and Exposition
GT2020
September 21-25, 2020, Virtual, Online

GT2020-14729

EFFECTS OF NON-AXISYMMETRIC VOLUTE ON ROTATING STALL IN THE VANELESS DIFFUSER OF A CENTRIFUGAL COMPRESSOR

Zitian NIU[1], Zhenzhong SUN[2], Baotong WANG[2], Xinqian ZHENG*[1,2]

[1] Turbomachinery Laboratory, State Key Laboratory of Automotive Safety and Energy
Tsinghua University, Beijing, 100084, China.

[2] Institute for Aero Engine
Tsinghua University, Beijing, 100084, China.
Email: zhengxq@tsinghua.edu.cn

ABSTRACT

Rotating stall is an important unstable flow phenomenon that leads to performance degradation and limits the stability boundary in centrifugal compressors. The volute is one of the sources to induce the non-axisymmetric flow in a centrifugal compressor, which has an important effect on the performance of compressors. However, the influence of volute on rotating stall is not clear. Therefore, the effects of volute on rotating stall by experimental and numerical simulation have been explored in this paper. It's shown that one rotating stall cell generates in a specific location and disappears in another specific location of the vaneless diffuser as a result of the distorted flow field caused by the volute. Also, the cells cannot stably rotate in a whole circle. The frequency related to rotating stall captured in the experiment is 43.9% of the impeller passing frequency (IPF), while it is 44.7% of IPF captured by three-dimensional unsteady numerical simulation, which proves the accuracy of the numerical method in this study. The numerical simulation further reveals that the stall cell initialized in a specific location can be split into several cells during the evolution process. The reason for this is that the blockage in the vaneless diffuser induced by rotating stall is weakened by the mainstream from the impeller exit to make one initialized cell disperse into several ones. The volute has an important influence on the generation and evolution process of the rotating stall cells of compressors. By optimizing volute geometry to reduce the distortion of the flow field, it is expected that rotating stall can be weakened or suppressed, which is helpful to widen the operating range of centrifugal compressors.

NOMENCLATURE

Q_{ref}	Mass flow rate at choke condition
Q	Mass flow rate
$\overline{P_s}$	Average static pressure
P_s	Static pressure
IPF	Impeller passing frequency
CFD	Computational fluid dynamics
V_s	Streamwise velocity
rev	Revolutions of impeller
P_r	Pressure ratio

Subscripts

1	Impeller inlet
2	Impeller outlet
3	Diffuser inlet
4	Diffuser outlet

1. INTRODUCTION

Centrifugal compressors are widely used in vehicle and marine turbochargers, industrial compressors and gas turbines. Therefore, the performance and stability of centrifugal compressor have been focused on by many researchers. Rotating stall is one of the well-known flow phenomena which can deteriorate compressors' performance and stable operating range [1]. The typical characteristic of rotating stall in compressor is that one or more stall cells rotate along the circumferential direction at a certain speed. The temporal scale of rotating stall corresponds to the impeller passing frequency (IPF) (generally 20%-80% of the IPF), and the spatial scale is related to the circumference circle length of the compressor casing [2].

Many researchers have conducted a lot of work on rotating stall of centrifugal compressors by experiments. As early as 1964, Jasen [3] observed the rotating stall phenomenon in vaneless diffuser by experiments and found that the initialization

*Corresponding author

of rotating stall in vanless diffuser was related to flow separation. In 1984, Fringe [1, 4] firstly explored the differences of the rotating stall in the impeller and vanless diffuser in the experiment and proposed the theoretical model based on the results. Subsequently, many scholars [5-7] explored the influence of diffuser geometric features, for example diffuser width and inlet shape, on the structure of rotating stall. In addition to using the traditional contact measurement method to study the rotating stall, some scholars [8-10] have developed Particle Image Velocimetry (PIV), which is a non-contacted measurement method to capture the flow field in detail, indicating that the stall cells can rotate stably under the axisymmetric flow field. Generally, the experiment can only obtain limited flow field information, but more details need to be shown by numerical simulation. Therefore, the research on the numerical simulation of three-dimensional flow field was developed gradually after the significant improvement of computing power in recent decades. The numerical simulation ten years ago mainly focused on one-dimensional and two-dimensional flow field [11, 12]. In 2012, Everitt [13] conducted a simulation of the rotating stall in the vaned diffuser and found that the rotating stall was caused by the flow separation, which was a result of the excessive attack angle around the leading edge of the blade tip in vaned diffuser. Bousquet [14] described the flow field with rotating stall at the inlet of the impeller by means of three-dimensional numerical simulation. Vagani [15] captured the rotating stall cells which could rotate at the inlet of impeller stably by means of the commercial software ANSYS-CFX. Filip [16] also used ANSYS-CFX to conduct unsteady numerical simulation based on an axisymmetric centrifugal compressor geometry. The results showed that the rotating stall cells rotated stably along with the circumferential position of the vanless diffuser, and the number of stall cells decreased along with the mass flow rate decreasing. Zhao [17] obtained the clear view of flow field including stable propagation of the rotating stall cells in the vaned diffuser, whose rotating frequency was 4.5% of the impeller passing frequency (IPF). The rotating stall can not only exist in a single component but also transfer from one component to another. Fujisawa and Ohta [18] found the transient process from diffuser stall to impeller stall. In addition to solving the traditional three-dimensional unsteady reynolds average Navier-Stokes (URANS) equations for simulation, with the improvement of computing power, researchers began to use the Detached-Eddy Simulation (DES) method to study the characteristics of rotating stall phenomenon. Ohta [19] and Fujisawa [20, 21] studied the mechanism of the rotating stall in the diffuser and impeller by DES and provided a quite detailed view of the flow field, in which the stall cells can rotate stably. However, due to the high requirement for the computing power in DES, researchers mainly prefer URANS for studying the rotating stall phenomenon.

The volute is an important component of a centrifugal compressor, which can cause the non-axisymmetric flow field. Many researches have focused on the effects of volute on the performance of centrifugal compressors. Zheng [22] studied the effect of non-axisymmetric volute on the performance of the centrifugal compressor, showing that the non-axisymmetric structure of the volute can reduce the compressor's efficiency by 4% and reduce the stable operation range of the compressor. To deal with the influence of non-axisymmetric flow field induced by the volute, Zheng [23], Sun [24] and Zhang [25] successively proposed the methods including optimization of volute geometry, the design of the asymmetric vaned diffuser, the match improvement of the distortions from impeller inlet and outlet, which can weaken the effects of the volute on performance degradation of compressor.

Previous studies mainly focused on the effect of axisymmetric flow field on the initialization of rotating stall, on the other hand, the researches on the effect of non-axisymmetric volute mainly focused on steady-state performance and stability boundary. However, the influence of non-axisymmetric volute on rotating stall phenomenon is not clear yet. This paper studied the effects of volute on rotating stall in the vaneless diffuser by experimental and numerical methods. The results are expected to guide the volute design.

2. METHODOLOGY

2.1 METHODOLOGY OF EXPERIMENT

2.1.1 CASE DESCRIPTION

The experiment in this paper adopts an in-house designed centrifugal compressor, which is composed of impeller, vaneless diffuser, and volute. The picture of the impeller is shown in Fig. 1, and the main specifications of the compressor are shown in Table 1.

Fig. 1 Impeller

Table 1 Main specifications of the investigated compressor

PARAMETERS	SYMBOLS	VALUES
Number of impeller blades	Z_I	24
Impeller outlet radius	r_2	50 mm
Leading edge hub radius	r_{1h} / r_2	0.26
Leading edge tip radius	r_{1t} / r_2	0.65
Rotational speed	N	70500 r/min
Diffuser inlet radius	r_3/r_2	1.10
Diffuser outlet radius	r_4/r_2	1.72
Diffuser width	b_3/r_2	0.07

2.1.2 EXPERIMENT SETUP

In order to obtain the overall performance characteristics of the compressor and the transient pressure characteristics of the flow field, the experiment was conducted by simultaneously measuring the steady pressure and temperature, as well as dynamic pressure. The scheme of the test rig is shown in Fig. 2. The air in ambient condition enters a huge plenum to maintain the stable temperature and pressure, which are taken as the inlet flow conditions of the compressor. The high-temperature and high-pressure gas flows into a turbine to drive a coaxial compressor at a specific speed. The flow rate of the compression system is measured by the flowmeter downstream of the inlet chamber, and the total pressure and temperature are measured at the compressor outlet. The compressor speed is measured by the magneto-resistive sensor at the compressor inlet. Several high response dynamic pressure transducers from Kulite are equipped inside the casing of centrifugal compressor, all of which have an uncertainty equal to ±0.1% of the full-scale range for pressure measurement. For more detailed information, six dynamic pressure transducers are arranged at the impeller inlet, and four dynamic pressure transducers are arranged at the diffuser inlet. The schematic of transducers setting is shown in Fig. 3.

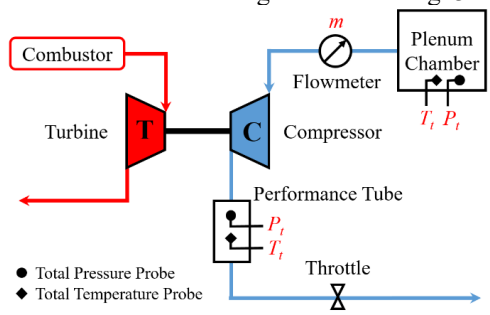

Fig. 2 The test rig

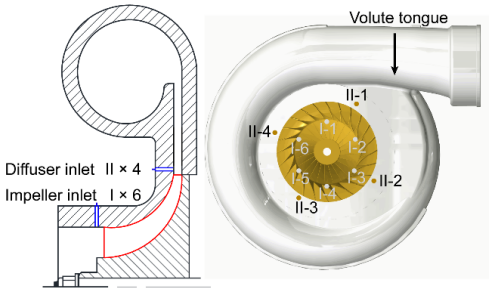

Fig. 3 Schematic of transducers setup

2.2 METHODOLOGY OF SIMULATION

ANSYS CFX17.1 platform is adopted for numerical simulation in this paper. TurboGrid is used to generate hexahedral mesh of impeller and vanless diffuser, and ANSYS ICEM is used to discretize the volute zone by tetrahedral mesh, CFX-Pre is used for setting the solver and boundary condition, and CFD-Post is used for post-processing.

2.2.1 GOVERNING EQUATION

The governing equation solved by the numerical simulation method is the three-dimensional compressible Unsteady Reynolds Average Navier-Stokes equation (URANS) as follows:

$$\frac{\partial \rho}{\partial t}+\nabla\cdot(\rho \boldsymbol{u})=0 \tag{1}$$

$$\frac{\partial}{\partial t}(\rho \boldsymbol{u})+\nabla\cdot(\rho \boldsymbol{u}\boldsymbol{u})=-\nabla p+\nabla\cdot\sigma \tag{2}$$

$$\frac{\partial}{\partial t}[\rho(e+\frac{1}{2}\boldsymbol{u}^2)]+\nabla\cdot[\rho(e+\frac{1}{2}\boldsymbol{u}^2)\boldsymbol{u}]=-\nabla\cdot(p\boldsymbol{u})+\nabla\cdot(\sigma\cdot\boldsymbol{u})+\nabla\cdot(\kappa\nabla T) \tag{3}$$

where ρ is density, $\boldsymbol{u}$ is velocity, p is static pressure, σ is viscous stress tensor, e is internal energy, κ is thermal conductivity, and T is static temperature. To make the equation enclosed, the following equations should be added:

$$\sigma=-\frac{2}{3}\mu(\nabla\cdot\boldsymbol{u})\mathrm{I}+2\mu\mathrm{E},\quad \mathrm{E}=\frac{1}{2}[\nabla\boldsymbol{u}+(\nabla\boldsymbol{u})^{\mathrm{T}}] \tag{4}$$

$$p=\rho R_g T,\quad e=c_v T \tag{5}$$

$$\mu=\text{constant},\quad \kappa=\text{constant},\quad c_v=\text{constant},\quad \gamma=\text{constant} \tag{6}$$

where μ is viscosity, I is unit tensor, E is strain rate tensor, R_g is gas constant, c_v is specific heat, and γ is isentropic coefficient.

2.2.2 DISCRETIZATION METHODS

The second-order Euler backward scheme is used in this paper for temporal discretization, which is an implicit scheme with second-order accuracy. As for the spatial discretization of convective terms, this study adopts the High-Resolution method, which can be considered to have second-order accuracy, which is recommended for unsteady simulation by the CFX manual.

2.2.3 TURBULENCE MODEL

In this study, the turbulence model of SST (shear stress transport) proposed by Menter [26] in 1994, was chosen. The main purpose of using the SST turbulence model is to solve the problem of numerical accuracy in the case of flow field with strong adverse pressure gradient and significant flow separation. In the SST model, the *k-ω* model is used near the wall to ensure the accuracy of the boundary layer simulating, while the *k-ε* model is used in the mainstream far away from the wall to reduce the calculating time. Since the object of this simulation is a centrifugal compressor, which has strong adverse pressure gradient along the streamwise direction and significant flow separation under conditions of rotating stall, the SST turbulence model is considered to be more suitable for this simulation.

2.2.4 CALCULATING DOMAIN AND MESH

The calculation domain of this simulation includes inlet pipe, impeller, vaneless diffuser, and volute, as shown in Fig. 4. For steady calculations, the volute exit is a common outlet pipe with constant cross-sectional area. As for the unsteady calculations, a nozzle is connected with the volute exit by a pipe with a shape line of cosine curve. Nozzle outlet needs to be choked to avoid the reflection from the given numerical boundary conditions on the calculation and enhance the stability of numerical simulation [27].

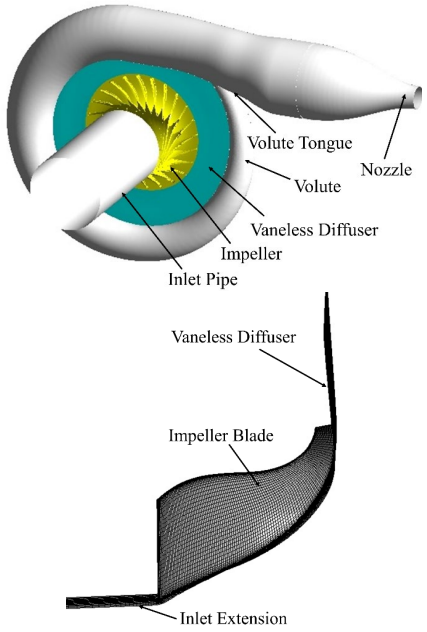

Fig. 4 Calculation domain and mesh

In this simulation, the hexahedral mesh is used for the flow passage in a whole circle of the impeller and diffuser. The single-passage mesh is shown in Fig. 4. The volute is calculated by tetrahedral mesh. The total mesh number of all domains is 17 million.

The thickness of the first mesh layer near the wall has a very important influence on accurately capturing the boundary layer. Generally, the dimensionless parameter y+ is used to indicate whether the thickness of the first layer of the grid is appropriate. Different turbulence models have different requirements for y+. For the SST turbulence model used in this simulation, the recommended value from the CFX technical manual is y+≤3 [28]. In order to meet the requirements of the SST turbulence model, the first grid thickness near the wall is set to be 0.001mm. Figure 5 shows the y+ distribution of all wall boundaries. It can be confirmed that the y+ value of all wall boundaries is less than 3, which meets the requirements of the SST turbulence model.

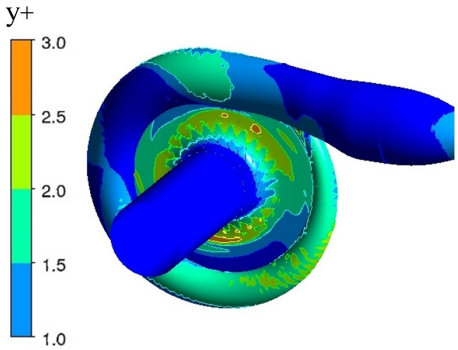

Fig. 5 y+ of the girds

2.2.5 BOUNDARY CONDITION

The inlet pipe, volute, and full-channel vaneless diffuser are calculated in a stationary frame, and the full circle passage of impeller calculation domains is calculated in a rotating frame. The rotor-stator interface in the steady-state calculation is set to be Stage Mixing-Plane. This method averages the parameters in the upstream side of the interface and transfers them to the downstream side of interface. As for the unsteady simulation, this paper adopts the Transient Rotor-Stator to consider the relative movement of mesh in rotating and stationary frames. In this way, the transient process can be better captured.

In the steady simulation, the axial uniform inlet flow with the total temperature and total pressure equal to 288.15K and 101325Pa are imposed as the inlet conditions. As for the outlet, the static pressure is continuously specified to obtain the steady performance map of the compressor. The wall is set to be adiabatic and non-slip, and the simulation convergence criterion is set to be that the RMS should be less than 1.0×10^{-6}.

In the unsteady simulation, the axial uniform inlet flow with the total temperature and total pressure equal to 288.15K and 101325Pa are also given as the inlet conditions. The atmospheric pressure is given at the domain outlet, and the compressor flow is controlled by the nozzle exit radius to achieve rotating stall condition. The wall is set to be adiabatic and non-slip, and the simulation convergence criterion is set to be that the parameters such as mass flow rate and pressure change periodically. After the unsteady simulation has reached convergence, another 8 impeller revolutions will be calculated, and the results are taken for analysis.

2.3 NUMERICAL SIMULATION VALIDATION

2.3.1 STEADY STATE RESULTS VALIDATION

In order to validate the accuracy of the simulation, the simulation results are compared with that of the experiment. The first step is the comparison of performance map to validate the accuracy of the numerical method to predict the overall performance of the compressor.

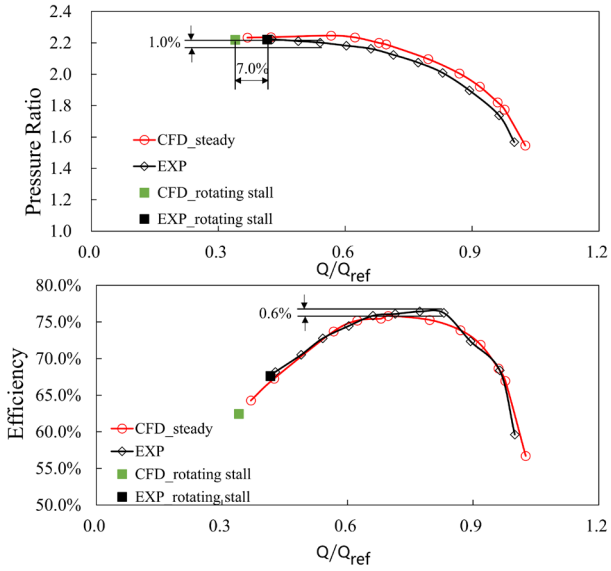

Fig. 6 Comparisons of experiment and CFD results

Comparisons of performance MAP between experiment and CFD are shown in Fig.6, the red line with a circle symbol in Fig. 6 represents steady simulation results, and the black line with diamond symbol represents experimental data. It can be seen from the figure that the errors of both pressure ratio and efficiency between CFD and experiment are within 1.0%, which proves that the predicted steady performance agrees well with that of the experiment. The black rectangle represents the rotating stall point measured in the experiment, and the green rectangle represents the rotating stall point by simulation. The relative error of rotating stall condition between CFD and experiment is about 7% in terms of mass flow rate.

2.3.2 TRANSIENT STATE RESULTS VALIDATION

In addition to comparing the steady results of overall performance map, the unsteady results also need to be compared to compare the simulated dynamic pressure signal with that of the test results. Figure 7 shows the comparison of unsteady pressure signals of experiment and unsteady CFD in the condition of rotating stall. The horizontal axis represents the impeller revolutions, while the vertical axis represents the normalized relative pressure. The numerical probes are arranged as shown in Fig.7. The numerical probes D-24, D-6, D-13, and D-19 are at the same locations with those of transducers in the experiment, as shown in Fig. 3. According to Fig. 7, it can be concluded that the pressure amplitudes and frequencies of CFD and experiment agree well with each other, and this validates the accuracy of the unsteady simulation.

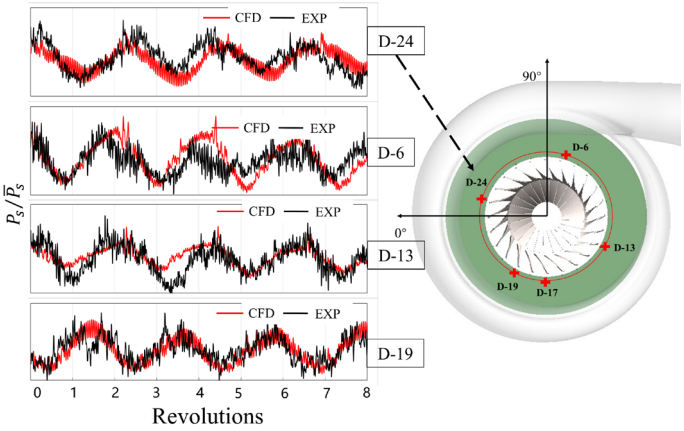

Fig. 7 Comparisons of experiment and CFD results of dynamic signal

3. RESULTS AND ANALYZATION

3.1 FORMATION OF ROTATING STALL CELLS IN DISTORTED FLOW FIELD CAUSED BY VOLUTE

In the previous researches, a rotating stall phenomenon in the vaneless diffuser of the compressor in this paper was found by analyzing the dynamic pressure data measured by pressure transducers, which is explained in the research of He [29] and Zou [30]. Fast Fourier Transformation (FFT) was performed on the signals of the transducer at the same location in both experiment and CFD, and the results are shown in Fig. 8. Both the experiment and CFD detected the generation of the rotating stall cells in a particular frequency, as shown in the purple box in Fig. 8. The frequency related to rotating stall detected in the experiment is 43.9% of IPF, while the frequency detected in the simulation is 44.7% of IPF. The error between the results of simulation and experiment is only 0.8%. Therefore, it is considered that the simulation can accurately reproduce the phenomenon of rotational stall formation in the experiment.

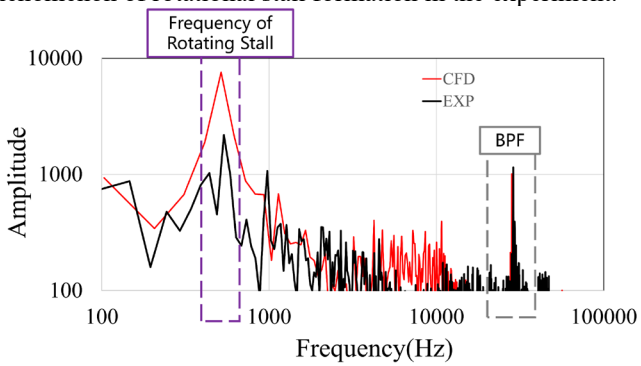

Fig. 8 Comparisons of experiment and CFD results of FFT

However, the generation position and evolution process of the rotating stall cells cannot be determined because the detailed flow field cannot be obtained from the experiment. Therefore, the numerical simulation is adopted as a supplementary to investigate the flow details in this study.

Fig. **9** shows the contour of streamwise velocity in a 15% spanwise section at T=0 rev, which is the time corresponding to the formation of the stall cells. As shown in Fig. 9, the region near the circumferential position 90° is defined as the area I, and the region near that of 180° is defined as area II. Moreover, the regions near 270° and 0° is regarded as area III and area IV, respectively, and the position of the volute tongue locates near the circumferential position of 120°.

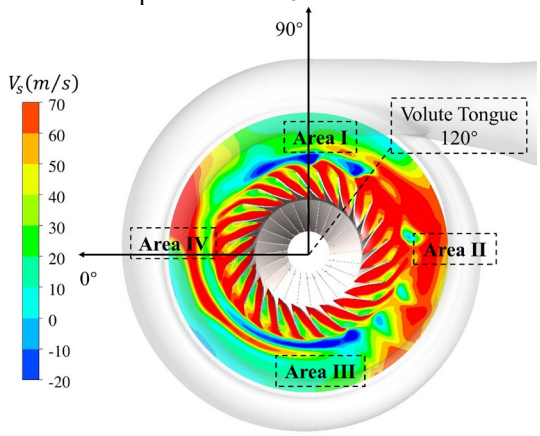

Fig. 9 Streamwise velocity at 15% span from hub to shroud at the time of T = 0 rev

In Fig. 10, the black rectangular is portrayed to mark a specific rotating stall cell in order to show the evolution process of the stall cells from the initialization to vanishment. At the time of T = 0 rev, the stall cell appears originally in area III. Then, at the time of T = 0.6 revs, the stall cells change from one to several

ones in area III and rotate downstream along with the circumferential position. At the time of T = 1.4 revs, the stall cells rotate through the area IV and reach the upstream of the volute tongue, while at the same time, the new stall cell starts to be generated in area III. Finally, at the time of T = 1.9 revs, the stall cells gradually disappear into the high velocity region at area II, which is near the downstream of the volute tongue.

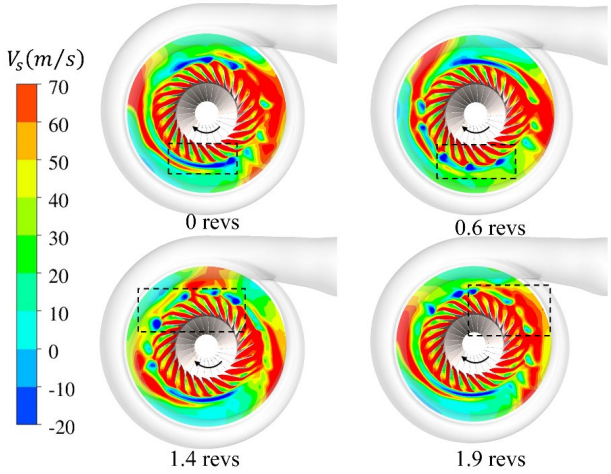

Fig. 10 Evolution of rotating stall cells

In the condition of axisymmetric flow field, the generation position of the rotating stall is not fixed in a particular circumferential position. Moreover, the stall cells can often rotate in a whole circle stably [17]. However, the research in this paper shows that the stall cell under the impact of the non-axisymmetric flow field caused by volute generates at a particular position of the area III (90 degrees downstream of the circumferential position of volute tongue). After that, the cell is split into several ones and rotates through the area IV and area I, then disappears in the area II. This phenomenon is quite different from the characteristics of the stall cells in the axisymmetric flow field.

In order to further understand the effects of volute on the formation of the rotational stall cell, a simulation without volute was also performed in this paper. Figure 11 shows the simulation results obtained at the condition of the same flow rate as that in Fig. 9. The numerical method and grid are chosen to be the same as the simulation with volute.

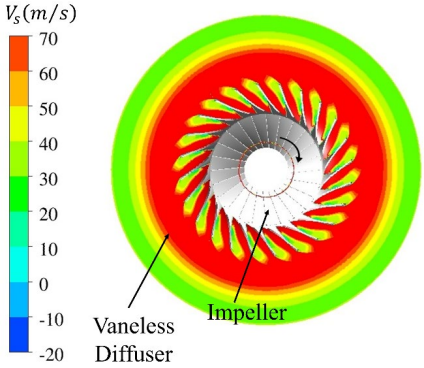

Fig. 11 Streamwise velocity of vaneless diffuser without volute

The contour of streamwise velocity in Fig. 11 shows that no rotating stall in the vaneless diffuser can be observed at the same flow rate with the previous simulation, and the flow is stable with axisymmetric flow field in the impeller and vaneless diffuser. The flow entering the vaneless diffuser is gradually decelerated along the radial direction, and no reverse flow and low momentum region can be found in the vaneless diffuser.

Based on the analysis above, it is concluded that the rotating stall in the compressor of this study is induced by the volute. The reason for its generation will be further analyzed.

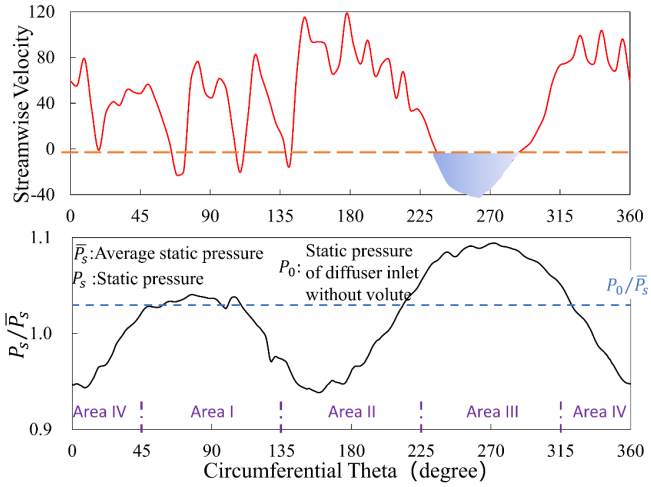

Fig. 12 Streamwise velocity and relative pressure distribution in a circumferential location

It is well known that the typical characteristic of the flow field under the impact of the non-axisymmetric volute is the non-axisymmetric pressure distortion along the circumferential direction. Due to the influence of the volute, area II in Fig. 12 is a low-pressure area and area III is a high-pressure area. This phenomenon has been proved in the research of Zheng [31, 32] and Sun [24]. The lower graph of Fig. 12 shows the relative static pressure distribution along the circumferential direction in the diffuser inlet at T = 0 rev. The blue dashed line $P_0/\overline{P}_s$ in this figure represents the normalized static pressure at the diffuser inlet by the static pressure of diffuser inlet at the same operation conditions with the simulations without the volute, which is almost uniform along with the circumferential position according to Fig. 11. Under the condition of uniform static pressure, there is no flow separation phenomenon in the vaneless diffuser of compressor, which has been proved in the streamwise velocity contour in Fig. 11. However, under the impact of non-axisymmetric flow field caused by volute, when the static pressure in some regions (such as area III) is higher than the value corresponding to this blue dashed line, which means the pressure of some impeller channel is higher and this induces unstable flow phenomenon such as rotating stall.

The time history of static pressure at the position of probe D17 (located in area III as shown in Fig. 7) is plotted in Fig. 13 with black line. The periodical pressure oscillation in Fig. 13 (black line) represents the generation and evolution process of the stall cells at this position. First, a stall cell initializes during

the process of pressure reaching at the peak condition, for example, from t=1.50 revs to t=2.00 revs. Then, when the pressure value becomes lower, the stall cell starts to evolve to make the D17 pressure signal show an irregular "sawtooth" oscillation. The evolution process will be described in the next section.

3.2 EVOLUTION PROCESS OF ROTATING STALL CELLS IN DISTORTED FLOW FIELD CAUSED BY VOLUTE

Under the condition of the axisymmetric flow field, the rotating stall cells can often stably rotate in a whole circle along the circumferential direction during the evolution process [10]. However, in this study, the rotating stall cell splits and vanishes under the impact of an axisymmetric distorted flow field caused by a volute.

Figure 13 shows the static pressure signal of probe D17 (shown in Fig. 7) at the position where the stall cell generates. T = 0 rev represents the time when a single stall cell begins to appear in area III. After that, it splits into several stall cells and rotates downstream as shown in Fig. 10, which corresponds to the area with many sawtooth-pressure oscillation signals enclosed by the red circle in Fig. 13. This "sawtooth" oscillation is related to the process where the stall cell splits into several cells, starting from the time of T = 0.3 revs. An enlarged view of this splitting process of stall cell is also shown in Fig. 13. After the "sawtooth" oscillation, the pressure signal stabilizes again after the time of T = 1.5 revs, indicating that at this moment, the stall cells move to the downstream along the circumferential direction without further splitting.

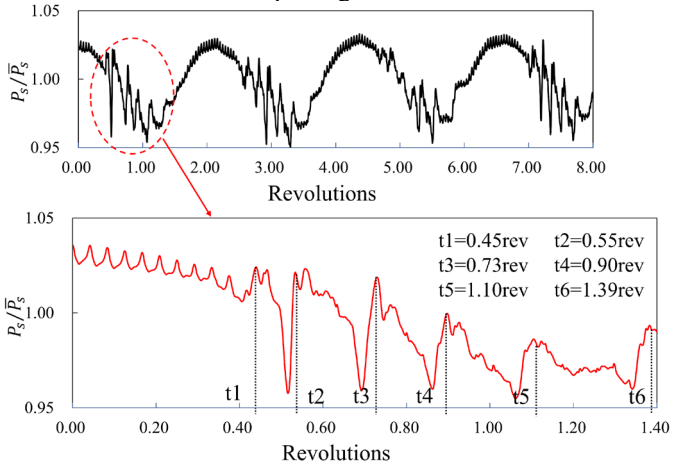

Fig. 13 Relative pressure signal at different time

Figure14 shows the contour of the streamwise velocity at different moments in Fig. 13. The asterisks in this figure show the position of the numerical probe D17 in Fig. 13. It is considered that each cycle of the pressure oscillates represents that a new stall cell passes through the probe position. At time t1, the probe D17 detects the pressure change for the first time, which implies that the first stall cell passes the position. Then, at time t2, the second pressure oscillation appears with the second stall cell passing this position. By counting the number of the pressure oscillation cycle from t1 to t6 in Fig. 13, it can be concluded that 6 stall cells pass through this position. When each split stall cell passes, a cycle of pressure oscillation will be caused, because the static pressure of the stall cell is quite different from the pressure of the surrounding fluid, and this causes a high amplitude pressure oscillation.

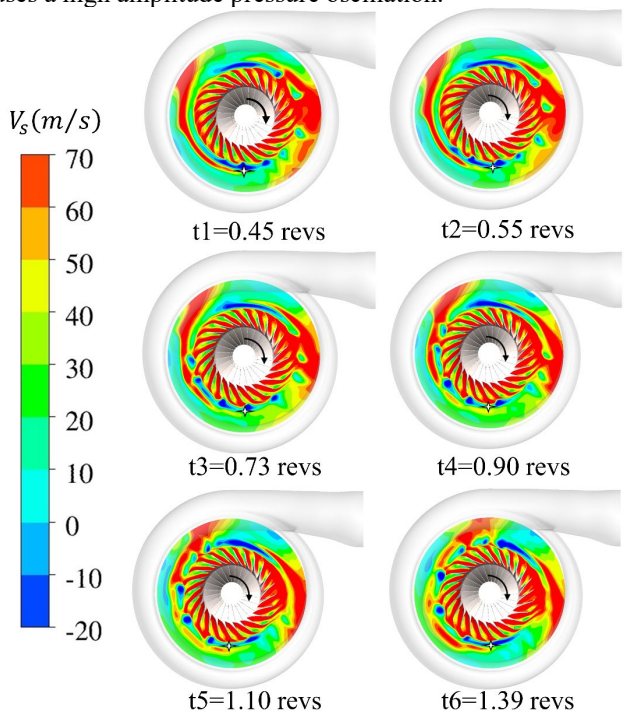

Fig. 14 Streamwise velocity contour at different time

Next，the mechanism of stall cell splitting will be analyzed. During the generation process of the stall cell, reversed flow with low momentum accumulates in area III. The velocity vectors in Fig. 15(a) show that the flow can only move in the tangential direction and this reverse flow region blocks the flow from the impeller exit into the diffuser, which is shown in Fig. 15(b). During this process, the situation is getting much worse, and the stall cell enlarges and continues to accumulate at this position. With the blockage becoming more and more severe, the fluid cannot flow into the region III to cause the static pressure rise in this region. With the impeller continues inputting fluid into the diffuser, the blocked area will be broken by the high velocity mainstream from the impeller exit to split the initialized stall cell into several ones. During this process, the static pressure in area III starts to decrease. As shown in Fig. 16(a), The red arrow represents the high-speed flow passing through stall cells, indicating that the fluid from the impeller has dispersed the stall cell, which is shown in Fig. 16(b).

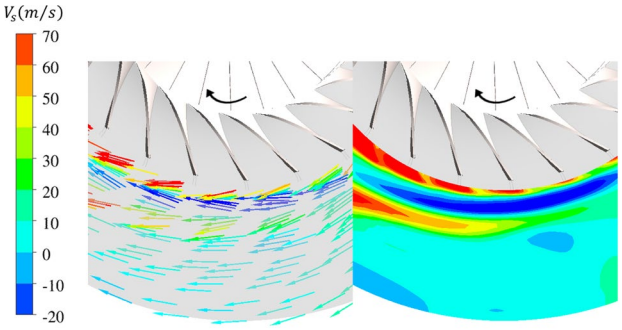

Fig. 15 (a) Velocity vectors and (b) Streamwise velocity contour during the generation process of rotating stall cells

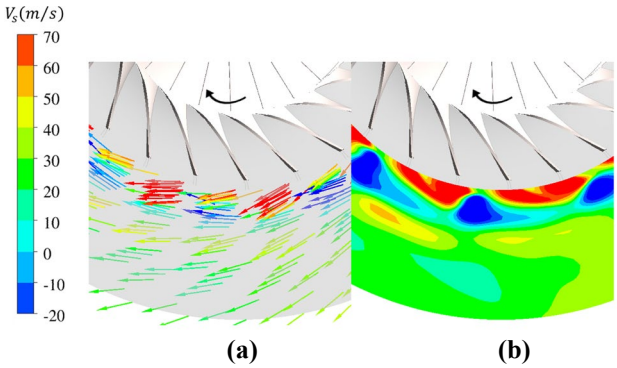

Fig. 16 (a) Velocity vectors and (b) Streamwise velocity contour during the evolution process of rotating stall cells

The stall cells cannot continue to rotate along the circumferential direction in a whole circle. After passing through area IV and area I, it will eventually disappear in area II and be merged into the mainstream. As shown in Fig. 17, the area marked by black oval corresponds to the position which locates at about 30 degrees downstream of the volute tongue. In this area, the rotating stall cells with accumulated reverse flow are merged into the mainstream. The reason for this is the low static pressure in this region as shown in Fig. 12. The flow velocity is greatly increased under the effect of the positive pressure gradient. At the same time, the back pressure of the local blade row in this region is very low, and this makes flows in this region work in a relatively stable condition.

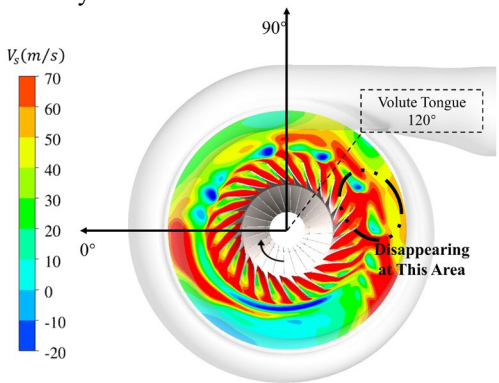

Fig. 17 Area of rotating stall cells disappearing

4. CONCLUSIONS

Rotating stall is one of the unstable flow phenomena which can deteriorate the performance and stable operation range of compressors. This paper studied the effects of the non-axisymmetry flow field caused by volute on the generation and evolution process of rotating stall in the vaneless diffuser by experimental and numerical methods. Conclusions could be drawn as follows:

(1) Under the distorted flow field induced by volute, the rotating stall is easy to be induced in the particular circumferential position of vaneless diffuser, which locates at 90 degrees downstream of the volute tongue along with the circumferential position. The stall cell disappears at a particular circumferential position, which locates at 30 degrees downstream of the volute tongue. The reason for the generation of the stall cell is that the blade row passes through the peak static pressure area of a distorted flow field caused by volute. This easily induces the flow instability because of the adverse pressure gradient. The reason for the disappearance of the stall cells is that the region locating at 30 degrees downstream of the volute tongue is a low-pressure region. The fluid flows along a positive pressure gradient with high velocity, and the back pressure of the blade row passing through this region is low enough to make them work in a relatively stable condition. The frequency captured from the unsteady numerical simulation is 44.7% of IPF, compared with that of the experiment equal to 43.9% of IPF.

(2) During the evolution process of the rotating stall cells, one stall cell can be split into several cells. The reason for this is that the mainstream with high velocity from the impeller exit breaks the blocking area caused by the stall cells which is the accumulation of reverse flow. Then the initialized stall cell disperses into several cells and rotates along the circumferential direction.

(3) The volute not only affects the performance of the centrifugal compressor but also has important impacts on the generation and evolution process of rotating stall. Therefore, it is expected to suppress the occurrence of rotating stall by optimizing the volute geometry to reduce pressure distortion along the circumferential direction in the vaneless diffuser, which is helpful to widen the operating range of centrifugal compressors.

ACKNOWLEDGMENTS

This research was supported by the National Science and Technology Major Project (2017-II-0004-0016), the National Natural Science Foundation of China (Grant No.51876097), and the Tsinghua University “Shuimu Tsinghua Scholar” Program.

REFERENCES

[1] Frigne, P., and Van Den Braembussche, R., 1984, “Distinction between Different Types of Impeller and Diffuser Rotating Stall in a Centrifugal Compressor with

Vaneless Diffuser," ASME Journal of Engineering for Gas Turbines and Power, **106**, pp. 468-474.
[2] Day, I. J., 2015, "Stall, Surge, and 75 Years of Research," Journal of Turbomachinery, **138**(1), 011001.
[3] Jansen, W., 1964, "Rotating Stall in a Radial Vaneless Diffuser," Journal of Fluids Engineering, Transactions of the ASME, **86**(4), pp. 750-758.
[4] Frigne, P., and Van Den Braembussche, R., 1985, "A Theoretical Model for Rotating Stall in the Vaneless Diffuser of a Centrifugal Compressor," Journal of Engineering for Gas Turbines and Power, **107**(2), pp. 507-513,.
[5] Kobayashi, H., Nishida, H., Takagi, T., and Fukushima, Y., 1990, "A Study on the Rotating Stall of Centrifugal Compressors. II-Effect of Vaneless Diffuser Inlet Shape on Rotating Stall," Japan Society of Mechanical Engineers, Transactions B, **56**, pp. 2646-2651.
[6] Jaatinen, A., Grönman, A., Turunen-Saaresti, T., and Röyttä, P., 2011, "Effect of Vaneless Diffuser Width on the Overall Performance of a Centrifugal Compressor," Proceedings of the Institution of Mechanical Engineers, Part A: Journal of Power and Energy, **225**(5), pp. 665-673.
[7] Ferrara, G., Ferrari, L., and Baldassarre, L., 2004, "Rotating Stall in Centrifugal Compressor Vaneless Diffuser: Experimental Analysis of Geometrical Parameters Influence on Phenomenon Evolution," International Journal of Rotating Machinery, **10**(6), pp. 433-442.
[8] Hayashi, N., Koyama, M., and Ishida, M., 2010, "Velocity Measurement by PIV of Radial Vaneless Diffuser under Rotating Stall Condition," Turbomachinery, **38**(4), pp. 215-226.
[9] Dazin, A., Cavazzini, G., Pavesi, G., Dupont, P., Coudert, S., Ardizzon, G., Caignaert, G., and Bois, G., 2011, "High-Speed Stereoscopic PIV Study of Rotating Instabilities in a Radial Vaneless Diffuser," Experiments in Fluids, **51**(1), pp. 83-93.
[10] Ohuchida, S., Kawakubo, T., and Tamaki, H., 2013, "Experimental Study of Rotating Stall in Vaneless Diffuser of a Centrifugal Compressor," ASME Paper No. GT2013-95468.
[11] Ljevar, S., De Lange, H., and Van Steenhoven, A., 2006, "Two-Dimensional Rotating Stall Analysis in a Wide Vaneless Diffuser," International Journal of Rotating Machinery, **2006**, pp. 1-11.
[12] Ljevar, S., De Lange, H., and Van Steenhoven, A., 2005, "Rotating Stall Characteristics in a Wide Vaneless Diffuser," ASME Paper No. GT2005-68445.
[13] Everitt, J. N., and Spakovszky, Z. S., 2013, "An Investigation of Stall Inception in Centrifugal Compressor Vaned Diffuser," Journal of Turbomachinery, **135**(1), 011025.
[14] Bousquet, Y., Binder, N., Dufour, G., Carbonneau, X., Roumeas, M., and Trebinjac, I., 2016, "Numerical Simulation of Stall Inception Mechanisms in a Centrifugal Compressor with Vaned Diffuser," Journal of Turbomachinery, **138**(12), 121005.
[15] Vagani, M., Engeda, A., and Cave, M. J., 2013, "Prediction of Impeller Rotating Stall Onset Using Numerical Simulations of a Centrifugal Compressor. Part I: Detection of Rotating Stall Using Fixed-Flow Transient Simulations," Proceedings of the Institution of Mechanical Engineers, Part A: Journal of Power and Energy, **227**(4), pp. 403-414.
[16] Filip, G., and Grzegorz, L., 2018, "Three-Dimensional Vaneless Diffuser Rotating Stall Numerical Study," ASME Paper No. GT2018-76716.
[17] Zhao, Y., Zhao, J., Wang, Z., and Xi, G., 2017, "Numerical Investigation of Diffuser Flow Field and Rotating Stall in a Centrifugal Compressor With Vaned Diffuser," ASME Paper No. GT2017-63913.
[18] Fujisawa, N., and Ohta, Y., 2017, "Transition Process from Diffuser Stall to Stage Stall in a Centrifugal Compressor with a Vaned Diffuser," International Journal of Rotating Machinery, **2017**, pp. 13
[19] Ohta, Y., and Fujisawa, N., 2014, "Unsteady Behavior and Control of Vortices in Centrifugal Compressor," Journal of Thermal Science, **23**(5), pp. 401-411.
[20] Fujisawa, N., Hara, S., and Ohta, Y., 2016, "Unsteady Behavior of Leading-Edge Vortex and Diffuser Stall in a Centrifugal Compressor with Vaned Diffuser," Journal of Thermal Science, **25**(1), pp. 13-21.
[21] Fujisawa, N., Inui, T., and Ohta, Y., 2019, "Evolution Process of Diffuser Stall in a Centrifugal Compressor with Vaned Diffuser," Journal of Turbomachinery, **141**(4), 041009.
[22] Zheng, X., Lin, Y., and Sun, Z., 2018, "Effects of Volute's Asymmetry on the Performance of a Turbocharger Centrifugal Compressor," Proceedings of the Institution of Mechanical Engineers, Part G: Journal of Aerospace Engineering, **232**(7), pp. 1235-1246.
[23] Zheng, X., Sun, Z., Kawakubo, T., and Tamaki, H., 2018, "Stability Improvement of a Turbocharger Centrifugal Compressor by a Non-Axisymmetric Vaned Diffuser," Journal of Turbomachinery, **140**(4), 041007.
[24] Sun, Z., Zheng, X., Linghu, Z., Kawakubo, T., Tamaki, H., and Wang, B., 2019, "Influence of Volute Design on Flow Field Distortion and Flow Stability of Turbocharger Centrifugal Compressors," Proceedings of the Institution of Mechanical Engineers, Part D: Journal of Automobile Engineering, **233**(3), pp. 484-494.
[25] Zhang, M., and Zheng, X., 2018, "Criteria for the Matching of Inlet and Outlet Distortions in Centrifugal Compressors," Applied Thermal Engineering, **131**, pp. 933-946.
[26] Menter, F. R., 1994, "Two-Equation Eddy-Viscosity Turbulence Models for Engineering Applications," AIAA Journal, **32**(8), pp. 1598-1605.
[27] Vahdati, M., Sayma, A. I., Freeman, C., and Imregun, M., 2005, "On the Use of Atmospheric Boundary Conditions

for Axial-Flow Compressor Stall Simulations," Journal of Turbomachinery, **127**(2), pp. 349-351.
[28] Menter, F. R., 2009, "Review of the Shear-Stress Transport Turbulence Model Experience from an Industrial Perspective," International Journal of Computational Fluid Dynamics, **23**(4), pp. 305-316.
[29] He, X., and Zheng, X., 2018, "Flow Instability Evolution in High Pressure Ratio Centrifugal Compressor with Vaned Diffuser," Experimental Thermal and Fluid Science, **98**, pp. 719-730.
[30] Zou, W., He, X., Zhang, W., Niu, Z., and Zheng, X., 2019, "Roles of Vanes in Diffuser on Stability of Centrifugal Compressor," Proceedings of the Institution of Mechanical Engineers, Part G: Journal of Aerospace Engineering, 0954410019844433.
[31] Zheng, X., Jin, L., and Tamaki, H., 2014, "Influence of Volute-Induced Distortion on the Performance of a High-Pressure-Ratio Centrifugal Compressor with a Vaneless Diffuser for Turbocharger Applications," Proceedings of the Institution of Mechanical Engineers, Part A: Journal of Power and Energy, **228**(4), pp. 440-450.
[32] Zheng, X., Jin, L., and Tamaki, H., 2013, "Influence of Volute Distortion on the Performance of Turbocharger Centrifugal Compressor with Vane Diffuser," Science China Technological Sciences, **56**(11), pp. 2778-2786.